scientific reports

Check for updates

OPEN

Formulation and evaluation of cetuximab functionalized phospholipid modified nanocrystals of paclitaxel for non-small cell lung cancer therapy

Manish Kumar[1,3], Pooja Goswami[2], Abhishek Jha[1,4], Manjit Manjit[1], Amol Parasram Satpute[1], Biplob Koch[2]✉ & Brahmeshwar Mishra[1]✉

Present work aims to prepare Soluplus stabilized, phospholipid-modified, and cetuximab-conjugated paclitaxel nanocrystals (NCs) as stable nanocarriers for targeted drug delivery. The NCs, prepared using concurrent antisolvent precipitation cum cold crystallization method followed by probe sonication, were found to be monodispersed particles with sub-200 nm size. The microscopic analysis uncovered rod and spherical anisotropy for Soluplus stabilized (PTX-NCs) and phospholipid modified (Lipid/PTX-NCs) nanocrystals, respectively. The formation of amorphous PTX-NCs and subsequent coating with phospholipid was confirmed by solid-state characterization using differential scanning calorimetry (DSC), X-ray diffraction (XRD), and Fourier transform Infrared Spectroscopy (FTIR). X-ray Photoelectron Spectroscopic (XPS) analysis, indicated successful conjugation of cetuximab on NCs surface. Lipid coating rendered a sustained drug release behaviour to NCs at physiological pH. In vitro cell line studies confirmed the improved cellular internalization and better apoptosis induction capability of NCs, consequently resulting in enhanced efficacy of PTX against A549 cancer cells. Moreover, in Benzo[a] pyrene-induced lung cancer model, Cmab/Lipid/PTX-NCs showed significant improvement in tumor inhibition potential in comparison to pure PTX. The prepared Cmab/Lipid/PTX-NCs also exhibited improved pharmacokinetics performance, avoided off-target distribution, and showed a reduction in systemic toxicity. The findings of this study indicate the promising potential of the prepared cetuximab-functionalized phospholipid-coated paclitaxel nanocrystals in lung cancer therapy.

Keywords Nanocrystals, Paclitaxel, Cetuximab, Lung cancer

Paclitaxel is a naturally derived tricyclic diterpenoid with potent anticancer activity against all types of cancers, specially, lung, breast, cervical, prostate, colorectal, gastric, ovarian, bone, and brain tumors[1,2]. However, the clinical application of its natural form has been limited by its physicochemical characteristics like low aqueous solubility, poor permeability, and p-gp efflux[3]. The paclitaxel structure lacks functional groups that can be used for chemical modification to improve its properties. This necessitated the search for a suitable approach for improving the physicochemical properties of paclitaxel and, thus, anticancer efficacy. Although various approaches like the use of co-solvents or surfactants have been reported for improving the physicochemical and pharmacological properties of paclitaxel[4]. These are associated with side effects or systemic toxicities. More specifically, Cremophor EL: ethanol (50:50 mixture) has been employed as a cosolvent system for formulation (Taxol or generic equivalents) for intravenous administration[5]. Though the idea was suitable for overcoming the limited solubility of paclitaxel, it was associated with toxicities like hyperlipidaemia, erythrocyte aggregation,

[1]Department of Pharmaceutical Engineering and Technology, Indian Institute of Technology (BHU), Varanasi 221005, Uttar Pradesh, India. [2]Genotoxicology and Cancer Biology Laboratory, Department of Zoology, Institute of Science, Banaras Hindu University, Varanasi 221005, Uttar Pradesh, India. [3]Amity Institute of Pharmacy, Amity University, Greater Noida 201308, India. [4]Department of Pharmaceutics, Dr. D. Y. Patil Institute of Pharmaceutical Sciences and Research, Pimpri, Pune 411018, Maharashtra, India. ✉email: biplob@bhu.ac.in; bmishra.phe@iitbhu.ac.in

hypersensitivity, sensory neuropathy, and neutropenia. Surfactant like Tween-80 has also been employed for improving drug solubility but are associated with hypersensitivity, peripheral neuropathy, and haemolytic activity[6]. Therefore, there is an urgent requirement of an alternating strategies that not only enhance the physicochemical properties and in-vivo efficacy of drug but also avoid serious and dose-limiting toxicities.

Recently, drug nanocrystals have been emerged as a potent nanocarrier with smaller size, high drug loading and greater structural stability[7–9]. Nanocrystals owing to their size can provide better antitumor effect via enhanced permeation and retention in the vicinity of the tumor. Nanocrystals can be administered as intravenous injection for drug delivery to cancer cells. However, nanocrystals can release drug rapidly in systemic circulation due to higher dissolution velocity, as predicted by the Ostwald-Freundlich and Noyes-Whitney principles[10]. This may result in off-target drug distribution to all major organs. Therefore, to control the drug release, prolong systemic circulation and specify drug delivery, surface modification of nanocrystals is required. Nanocrystals are usually stabilized using polymers or surfactants that adsorb on nanocrystals surface to provide stabilization via steric or electrostatic hinderance[11]. Besides this, proteins and lipids have been also explored for nanocrystals stabilization[12,13]. Nanocrystals can be surface coated with lipid materials to improve stability and prolong systemic circulation[14]. Lipid-coated nanocrystals can further be utilized to obtain a ligand-functionalized shell with NCs core providing combined advantage of high payload, good stability and selective delivery to target site, thereby avoiding off target distribution and minimizing systemic side effects related to anticancer drugs.

The aim of the present work was the formulation of lipid-coated nanocrystals for improved delivery of paclitaxel (PTX) (Illustration in Figure S1 of supplementary file). First, the NCs were prepared using Soluplus as a stabilizer. Soluplus is an amphiphilic polymer with solubility enhancement potential that can be used for the preparation of drug nanocrystals with hydrophilic surfaces. Prepared nanocrystals were then surface-modified with lipid materials consisting of hydrogenated Soy phosphatidylcholine (HSPC), Chol, and TPGS. HSPC was the phospholipid used to coat the hydrophilic surface of nanocrystals, Chol stabilized the lipid coating while TPGS provided a stealth layer, together responsible for prolonging the systemic circulation. Also, TPGS offers inhibition of p-glycoprotein (efflux pump) and thus can avoid the occurrence of multidrug resistance (MDR) in tumor cells. The Lipid-nanocrystals were surface-functionalized with targeting moiety to specify the drug delivery to cancer cells. Cetuximab was used for surface-functionalization that aided in targeted delivery via receptor-mediated endocytosis.

Experimental

Materials

Paclitaxel (USP, 98–100%) was obtained as gift sample from MSN Laboratories Pvt. Ltd., Telangana, India. The gift sample of Soluplus was received from BASF, India. Hydrogenated Soyphosphatidylcholine (HSPC) was gift sample obtained from Lipoid, GmBH. Vitamin E-TPGS was free sample gifted by Antares Health Products, St. Charles, USA. Cholesterol extrapure AR, 99% (Chol), Succinic anhydride (SA), 1-(3-Dimethylaminopropyl)−3-ethylcarbodiimide hydrochloride (EDC) and N, 4-Dimethylaminopyridine (DMAP) were purchased from SRL Pvt. Ltd., India. All solvents used were HPLC grades.

The A549 cell line, which originates from lung carcinoma was acquired from the National Centre for Cell Science (NCCS) situated in Pune, India. Genetics Biotech Asia Pvt. Ltd. supplied the necessary laboratory materials, such as DMEM (Dulbecco's Modified Eagle Medium) and 12-well cell culture plates. Procurement of T-25 flasks and 96-well plates was by Eppendorf. Penicillin–streptomycin, Trypsin–EDTA, and Fetal Bovine Serum (FBS) were supplied by Gibco, New York. Hoechst 33342 were purchased from Realgene, Italy. Phosphate Buffer Saline (PBS) of high-quality grade, MTT, RNase, and propidium iodide were obtained from SRL, India. JC-1 dye was purchased from Cayman Chemical, USA.

Preparation of lipid-nanocrystals of paclitaxel

The preparation of lipid nanocrystals was done in three steps, i.e., a) preparation of polymeric nanocrystals, b) formation of lipid film, and c) rehydration of lipid film with nanocrystals. The drug nanocrystals were first prepared by concurrent antisolvent precipitation cum cold crystallization method followed by probe sonication. Soluplus (1% w/v) was employed for stabilizing paclitaxel nanocrystals (PTX-NCs). The organic phase of ethanol (1 ml) containing drug (20 mg) was added drop wise to 1% (w/v) aqueous Soluplus solution (10 ml) using 1 ml syringe (24 gauze needle), maintained at 2000 rpm on ice cold water, using magnetic stirrer (C-MAG HS 7, IKA India Private Limited). The nanosuspension was then probe sonicated (UP50H, Hielscher Ultrasound Technology) at 60% amplitude (6 mm probe) for 10 min in 3-s ON and 2-s OFF cycle on ice bath. Resultant nanocrystals were further stirred for 6 h at room temperature, stored overnight at 4 ℃ undisturbed, and collected by ultra-centrifugation (Optima XPN-100 Ultracentrifuge) at 50,000 rpm for 30 min at 4 ℃.

For the preparation of lipid-nanocrystals (Lipid/PTX-NCs), 60 mg HSPC, 30 mg Chol, and 15 mg TPGS were dissolved in 2:1 v/v of chloroform and methanol mixture. The organic phase was evaporated at reduced pressure using rotary evaporator at 60 °C to form a thin film. The dry film was re-hydrated with 5 ml of nanocrystals suspension (equivalent to 100 mg of dry NCs) and stirred for about 6 h at 25 ℃[15]. The temperature of the resultant suspension was then reduced to 4 °C using an ice bath under continuous stirring. The cold suspension was then sonicated for 10 min at 45% amplitude using a 6 mm probe (3-s ON and 2-s OFF cycle) in an ice bath. The suspension was then stored overnight at 4 °C and collected by centrifugation at 12,000 rpm for 30 min. The sediment was redispersed in distilled water. The obtained Lipid/PTX-NCs were lyophilized (Freeze dryer, Alpha 1–2 LDplus Martin Christ, Gefriertrocknungsanlagen GmbH, Germany) and stored at 4–8 °C until further use.

For the preparation of targeted lipid-nanocrystals, 7.5 mg of TPGS was replaced by synthesized TPGS-COOH (detail in supplementary; Table S1)[16]. The redispersed purified Lipid/PTX-NCs were incubated with NHS and EDC for 30 min to activate TPGS-COOH, followed by the addition of Cetuximab (2 mg for 75 mg of Lipid/PTX-NCs) at 4 ℃. The conjugation between amine-terminal of cetuximab and activated TPGS-COOH

was allowed to occur at 200 rpm for 6 h. The resultant targeted lipid nanocrystals (Cmab/Lipid/PTX-NCs) were then washed, lyophilized, and stored at 4–8 °C until further use. For the preparation of coumarin-6 (C6) equipped formulation, 1 mg of C6 was used along with 20 mg PTX during the preparation of NCs.

Characterization of nanocrystals

Particle size, polydispersity index (PDI), zeta-potential, drug payload and yield

Hydrodynamic size, polydispersity index (PDI), and zeta-potential of PTX-NCs, Lipid/PTX-NCs, and Cmab/Lipid/PTX-NCs were determined by photon correlation spectroscopy (PCS) using Malvern Zetasizer (v7.13, Malvern Panalytical Ltd., UK). The drug payload and yield were determined using HPLC (HPLC, Shimadzu, Japan) equipped with a Waters-1525 binary HPLC pump (Waters, USA), rheodyne-7725i manual injector (Waters, USA), and Waters-2998 photodiode array detector (Waters, USA). A reverse phase C18 column (150 mm length, 4.6 mm diameter, and 3.5 µm particle size) and mobile phase composed of Acetonitrile: MilliQ water (60:40) was used to elute the analyte at a flow rate of 1 ml min^{-1}. The analysis was done at 229 nm wavelength[14]. For this, the known weight of nanocrystals was added to known volume of methanol, vortexed for 5 min and sonicated for 15 min to disintegrate the intact nanocrystals and obtain free drug in methanol. Then, obtained solution was centrifuged at 15,000 rpm to collect the supernatant used for drug quantification by HPLC method. The drug payload and yield were the calculated following below formulae:

Payload (%) = (Drug in nanocrystals weight/ weight of nanocrystals used) × 100.

Yield (%) = (Total weight of nanocrystals obtained/ total weight of solid i.e., drug + stabilizer + surface modifier used to formulate the nanocrystals) × 100.

Stability study

To evaluate the stability of nanocrystals, lyophilized nanocrystals were stored at 4 °C for 6 months. Hydrodynamic size, PDI, and zeta-potential were recorded at predefined time intervals (0, 0.5, 1, 2, 3, and 6 months) to assess the stability of nanocrystals[17,18].

Microscopic measurements

The size and morphology of nanocrystals were investigated using electron microscopy. For TEM analysis (TechnaiG2 20 TWIN, FEI, USA), 20 × diluted sample was cast on a carbon-coated copper grid and air dried. For preparing the sample for SEM, a single drop of 20 × diluted sample was dropped onto the glass slide and vacuum dried at 25 °C. The prepared slide was gold coated using a sputter coater (DSR1) for 120 s prior to SEM analysis (EVO MA15/18, Carl Zeiss Microscopy). The surface characteristics like shape and smoothness was also observed under scanning probe microscope (SPM, NTEGRA Prima, NT-MDT Service and Logistics Ltd) and analysed using Nova Powerscript 3.4.0 rev 16,681 software.

Solid state characterization

PTX-NCs, Lipid/PTX-NCs and Cmab/Lipid/PTX-NCs were also studied by various spectroscopic techniques including; Fourier-transform infrared (FT-IR), powder X-ray diffraction (XRD), and differential scanning calorimetry (DSC). The FTIR study was conducted using SHIMADZU 8400 S, Tokyo, Japan. For this, the pellets of pure PTX, Soluplus, SPPM (pure PTX and Soluplus as physical mixture), PTX-NC, Lipid/PTX-NCs and Cmab/Lipid/PTX-NCs were individually prepared with KBr (1:5) using hydraulic press and the scanning was done between 4000 cm^{-1} to 600 cm^{-1} at a resolution of 4 cm^{-1} at a rate of 64 accumulation per min. For confirming the conversion of crystalline drug to amorphous nanocrystals (PTX-NC), lipid coated crystals (Lipid/PTX-NCs) and Targeted crystals (Cmab/Lipid/PTX-NCs), XRD study was done. The diffraction pattern was obtained using Rigaku Miniflex 600 powder x-ray diffractometer equipped with a D/teX Ultra detector and measurements were set to step size of 0.02° at the scan rate of 5° per min over 2θ of 5–50°. The DSC study was performed at a heating rate of 20 ℃/min over temperature range − 25 −300 ℃ using Shimadzu DSC-60 Plus.

Surface chemistry and degree of conjugation

The elemental composition of Lipid/PTX-NCs and Cmab/Lipid/PTX-NCs was identified using XPS (K-Alpha model, Thermo Fisher Scientific) over 100–700 eV binding energy. The Bradford assay was performed to determine the degree of conjugation of cetuximab on Cmab/Lipid/PTX-NCs surface[19]. Stock Bovine serum albumin (BSA) was used as a standard protein to plot the calibration curve. For this, definite concentrations of BSA were incubated at + 37 °C for 5 min with Bradford's reagent that resulted in color change. The absorbance of BSA bound reagent was measured at 595 nm and calibration curve was plotted, later used for determining the degree of cetuximab conjugation on nanocrystals surface. For cetuximab quantification, washed Cmab/Lipid/PTX-NCs were incubated with Bradford's reagent for 5 min, absorbance measured and then amount quantified using the standard calibration curve.

In vitro drug release

The release study of pure PTX, PTX-NCs, Lipid/PTX-NCs and Cmab/Lipid/PTX-NCs was performed by dialysis method. Since PTX has a poor aqueous solubility, 0.5% (w/v) Tween-80 was included in acceptor compartment to maintain the sink condition. In brief, sample dispersed in 1 mL of PBS (pH 7.4) were sealed in a dialysis bag (8–14 kDa, HiMedia Laboratories Pvt. Ltd., Mumbai, India). Afterward, the dialysis bags were immersed in beaker with 20 mL of acceptor media maintained at 37 °C and stirring rate of 100 rpm. At fixed time points (0, 2, 4, 6, 12, 24, and 48 h), 1 mL of aliquot was withdrawn and replaced with fresh PBS. PTX concentration was determined by HPLC method.

In vitro cell lines studies

Cell line maintenance

The A549 cell line, derived from lung carcinoma, was grown in a CO_2 incubator with controlled temperature and humidity at 37 °C. The cells were cultured in DMEM supplemented with FBS (Fetal Bovine Serum) and a penicillin–streptomycin solution, providing them with essential nutrients and protecting against contamination. Once the cell culture reached a confluency of 70–80%, the cells were detached from the culture surface using a 0.25% trypsin EDTA solution, enabling their utilization in further experimental procedures.

In vitro cytotoxicity assay

The cytotoxicity of pure PTX, PTX-NCs, Lipid/PTX-NCs and Cmab/Lipid/PTX-NCs was assessed on the A549 cell line using the MTT (3-(4, 5-dimethylthiazolyl-2)−2, 5-diphenyltetrazolium bromide) assay. In a 96-well cell culture plate, 7000 cells were seeded in each well and left to adhere overnight. Subsequently, the cells were exposed to different concentrations of the compounds, ranging from 0.01 µg/ml to 20 µg/ml and incubated for 48 h. After the incubation period, the culture media was removed, and MTT-containing medium was added to each well. Following a 2 h incubation, the MTT-containing medium was replaced with 100 µl of DMSO in each well. The plate was further incubated for 30 min to dissolve the formazan crystals. Finally, using a microplate reader (Bio-Rad, USA), the absorbance was measured at 570 nm to evaluate the cytotoxic effects of the tested compounds. The percentage cell viability in each well was calculated using the formula;

Percentage cell viability (%) = (Absorbance of sample at 570 nm) / (Absorbance of control at 570 nm) × 100.

Nuclear morphological assessment through Hoechst 33342 /PI dual staining

Further, to investigate the effect of pure PTX, PTX-NCs, Lipid/PTX-NCs and Cmab/Lipid/PTX-NCs on nuclear morphology and condensation, Hoechst 33342 /PI dual staining were done. For this, approximately 3×10^4 cells were seeded in 12- well cell culture plate with 10% FBS and DMEM alongwith pen-strep antibiotic solution incubated in 5% humidified CO_2 incubator for growth and adherence. After attaining proper morphology, cells were treated with all above samples at IC_{50} concentration of Cmab/Lipid/PTX-NCs, and incubated for 48 h. Afterward, spent media were discarded, washed with PBS and then staining were done with Hoechst 33342 (10 µg/ml) and PI (5 µg/ml) and images were taken through fluorescence inverted phase contrast microscope (EVOS FL, Life technologies, India) at 400X magnification.

Mitochondrial membrane potential study through JC-1 staining

Alteration of mitochondrial membrane potentials is directly linked to ROS generation and cell death[20]. Mitochondria depolarization is a significant response of anticancer drug and an indirect indicator of drug internalization and its intracellular concentration. The commonly used dye JC-1 is used to assess the mitochondrial depolarization which gives red fluorescent J-aggregates (polarized) and green fluorescent J-monomers (depolarized). Briefly, 3×10^4 cells were seeded in 12- well cell culture plate which were supplemented with DMEM and 10% FBS and left it for adherence overnight. Thereafter, cells were exposed with or at IC_{50} concentration of Cmab/Lipid/PTX-NCs for pure PTX, PTX-NCs, and Lipid/PTX-NCs, then incubated for 48 h. Exhausted media were discarded and then stained with cationic JC-1dye (1 µM) and incubated for 15 min. Images were captured through inverted fluorescence phase contrast microscope (EVOS FL, Life technologies, India) at 400 X magnification.

Cellular uptake

Cellular uptake of free coumarin-6 (C6), C6-PTX-NCs, Lipid/C6-PTX-NCs and Cmab/Lipid/C6-PTX-NCs was investigated in A549 cells. Briefly, 30×10^3 A549 cells were seeded on coverslip in 12-well cell culture plate with DMEM alongwith 10% FBS and incubated for 12 h in 5% humidified CO_2 incubator. After incubation, spent media were discarded and counterstaining were done with DAPI stain. Images were captured through inverted fluorescence phase contrast microscope (EVOS FL, Life technologies, India) at 400 X magnification.

Cell cycle analysis

The cell cycle arrest by PTX is induced in G2/M phase to avoid cell proliferation. The enhanced intracellular availability of PTX in cells is responsible for cell cycle arrest in the G2/M phase. To investigate the role of pure PTX, PTX-NCs, Lipid/PTX-NCs and Cmab/Lipid/PTX-NCs in cell-cycle delay or growth arrest, cell cycle analysis study was done through flowcytometry. For this, 80,000 cells were seeded in 6- well cell culture plate alongwith DMEM and 10% FBS and incubated overnight in 5% humidified CO_2 incubator for growth and adherence. Thereafter, cells were exposed with PTX, PTX-NCs, Lipid/PTX-NCs and Cmab/Lipid/PTX-NCs at the IC_{50} concentration of Cmab/Lipid/PTX-NCs and then incubated for 48 h in 5% humidified CO_2 incubator. After incubation cells were harvested with the help of 0.5M EDTA solution and then centrifuge at 3000 rpm for 10 min. Subsequently, supernatant was discarded and then cells were fixed with 80% ethanol for overnight. Thereafter, cells were centrifuged at 3000 rpm for 7 min and supernatant were discarded and then cells were stained with RNase and propidium iodide and gave incubation for 15 min and then went for analysis through Flowcytometer (Cytofelx Beckman Coulter).

In vivo studies

All experimental protocols were approved by Institutional Animal Ethics Committee (IAEC) (Approval number: IIT(BHU)/IAEC/2024/I/009). All in vivo experiments were carried out in accordance with the guidelines of CPCSEA (a Committee for the Purpose of Control and Supervision of Experiments on Animals, Regd. No. 2123/GO/Re/S/21/CPCSEA). The methods were reported in accordance with ARRIVE guidelines.

Animals: Healthy mice (Swiss-albino, male, 20–25 g) were used for the experiment, maintained at 22 ℃ on 12-h light/dark cycle and fed standard pellet diet and water ad libitum.

Lung cancer model development:B(a)P (50 mg/kg) in corn oil was administered by oral gavage at a dose of twice a week (Day 0, 3, 7, 10, 14, 17, 21, 24, 28) for 4 weeks to induce the lung cancer[21].

Formulation: To administer pure PTX as positive control, PTX was dissolved in Kolliphor EL (Sigma Aldrich, St. Louis, MO) and ethanol mixture (1:1) and diluted with PBS (sterilized by filtration through 0.2 µm filter) to obtain 2 mg/ml PTX solution. The nanocrystals were also suspended in PBS to the same concentration for intravenous administration in the lateral tail vein.

Tumor regression, histological assessment and survival analysis

For in-vivo study, 5 groups (n = 6 mice with lung cancer) were used, intravenously (vein of the tail) administered with pure PTX, PTX-NCs, Lipid/PTX-NCs, and Targeted Lipid/PTX-NCs. One group was treated with saline solution (negative control). The animals were given treatment at a dose of 10 mg/kg of equivalent PTX twice a week for a total of three weeks. The weight of the mice was recorded at predetermined time intervals. At the end, animals were euthanized via intramuscular injection of high dose of ketamine (300 mg/kg) and xylazine (30 mg/kg) cocktail, to collect lung samples dehydrated with 95% ethanol and fixed in 10% formalin for histological study. For survival analysis, mice with lung cancer were divided into five groups (n = 6) and treated with normal saline (control), pure PTX, PTX-NCs, Lipid/PTX-NCs, and Targeted Lipid/PTX-NCs for three weeks. The mice were housed for 120 days, and individual death count was recorded throughout the study period. The mean survival of each group was determined by the Kaplan-Mier survival plot compared to normal healthy animals and saline-treated tumor-bearing mice.

Pharmacokinetics and biodistribution study

For the pharmacokinetics and biodistribution study, male mice were divided into four groups (n = 18). The treatment was given by intravenously administrating pure PTX, PTX-NCs, Lipid/PTX-NCs, and Cmab/Lipid/PTX-NCs at an equivalent dose of 10 mg/kg PTX. At fixed time points (0.5, 1, 3, 6, 12, and 24 h), three mice were used to collect the blood samples, and then euthanized for all major organs including liver, lung, heart, spleen, kidney and brain. The organs were weighed, resuspended in ACN (volume equal to twice the weight), and homogenized (high-speed homogenizer IKA T10 Basic ULTRA-TURRAX, Germany). Blood samples collected in EDTA tubes were used for separating plasma after centrifugation at 10,000 rpm for 10 min. Then, tissue and plasma (200 µL) were incubated for 10 min using ultrasonic bath, and added with docetaxel (15 µL) as internal standard. Each sample was vortexed for 1 min followed by incubation for 5 min at RT and vortex for 5 min to allow the extraction of PTX. After centrifugation at 10,000 rpm for 5 min, the supernatant was collected, and analyzed by HPLC.

Statistics

Experiments were performed in triplicates and data were presented as mean values ± SD. Statistical analyses were carried out using the GraphPad Prism 9.0.0 (GraphPad Software, San Diego, CA, USA). For determining the statistical significance among groups, unpaired two-tailed Student's t test, one-way ANOVA and two-way ANOVA were applied. Values with $p < 0.05$ (*), $p < 0.01$ (**), $p < 0.001$ (***), and $p < 0.0001$ (****) are considered significant, while $p > 0.05$ (ns) considered non-significant.

Results and Discussions

A preliminary optimization study was conducted for the preparation of PTX nanocrystals, as described in Table 1. The objective was to obtain PTX-NCs with a size less than 200 nm, PDI < 0.3, and maximum possible drug payload. The study included the selection of solvent, stabilizer type, stabilizer concentration, PTX amount, and antisolvent-to-solvent ratio. Methanol, ethanol, DCM, ethyl acetate, and DMSO were selected as organic solvents for preliminary screening due to PTX solubility in these solvents and co-solvency with antisolvent phase, i.e., water. The nanocrystals prepared using methanol and ethanol were smaller in size than DCM, DMSO, and ethyl acetate. This could be due to the higher diffusion rate of methanol and ethanol in water, which leads to rapid distribution of the organic phase to the aqueous phase[22]. This results in crystal nuclei forming, which are stabilized with polymer Soluplus to form stable nanocrystals. However, the difference between methanol and ethanol was not significant. Thus, ethanol attributed to their lower toxicity was selected as suitable solvent over methanol for further study.

Another important factor in nanocrystal formulation is the type and concentration of the stabilizers. The stabilizer was chosen from hydrophilic polymer, amphiphilic polymer, and surfactant. Interestingly, amphiphilic polymers produced nanocrystals of a lower size. In contrast, hydrophilic polymers and surfactants in the antisolvent phase produced larger sized crystals than amphiphilic polymers. This could be due to the drug's increased solubility in antisolvent, reducing the difference between the solvent and antisolvent phases, which in turn reduces the precipitation rate and promotes crystal formation as a result of Ostwald ripening. Furthermore, the concentration of stabilizer was closely related to particle size, which decreases up to a point with stabilizer concentration before resulting in larger particles at higher concentrations. The amount of PTX was another critical factor determining nanocrystals size. 20 mg PTX in 1 ml ethanol was chosen for the study since a lower amount although reduced the particle size but also decreased the drug payload. PTX, when used in higher amounts than 20 mg, resulted in larger crystals, probably due to the creation of a higher level of supersaturation, which slowed the diffusion rate between solvent and antisolvent, resulting in particle collision to give larger crystal nuclei[23].

Solvent	Stabilizer	Stabilizer concentration (% w/v)	PTX (mg) in 1 ml solvent	Antisolvent–solvent ratio	*Hydrodynamic Particle size (nm)	PDI	*Zeta potential (mV)	*Drug payload (%)
Ethanol	Soluplus	1	20	20:1	81 ± 27	0.27	−10.93 ± 1.15	22.73 ± 1.46
Methanol	Soluplus	1	20	20:1	74 ± 11	0.32	−11.54 ± 1.04	-
DCM	Soluplus	1	20	20:1	369 ± 19	0.29	−7.28 ± 1.16	-
EA	Soluplus	1	20	20:1	427 ± 27	0.31	−4.23 ± 1.11	-
DMSO	Soluplus	1	20	20:1	372 ± 32	0.35	−5.32 ± 1.09	-
Ethanol	HPMC	1	20	20:1	252 ± 35	0.23	−6.34 ± 1.75	-
Ethanol	TPGS	1	20	20:1	137 ± 28	0.15	−7.24 ± 1.07	
Ethanol	Captisol	1	20	20:1	213 ± 32	0.21	−7.93 ± 1.43	-
Ethanol	Pluronic F68	1	20	20:1	325 ± 21	0.35	−8.26 ± 1.65	-
Ethanol	Pluronic F127	1	20	20:1	367 ± 25	0.42	−8.73 ± 1.82	-
Ethanol	Tween 20	1	20	20:1	397 ± 31	0.27	−7.13 ± 1.24	-
Ethanol	Tween 80	1	20	20:1	426 ± 37	0.23	−5.27 ± 1.57	-
Ethanol	Soluplus	0.5	20	20:1	129 ± 12	0.41	−9.20 ± 1.06	21.35 ± 1.37
Ethanol	Soluplus	2.5	20	20:1	121 ± 7	0.25	−7.33 ± 2.15	20.34 ± 1.19
Ethanol	Soluplus	5	20	20:1	165 ± 34	0.32	−8.63 ± 1.18	16.83 ± 2.05
Ethanol	Soluplus	1	20	5:1	172 ± 19	0.13	−8.05 ± 1.09	-
Ethanol	**Soluplus**	**1**	**20**	**10:1**	**109 ± 5**	**0.10**	**− 10.31 ± 1.82**	**25.63** ± 1.21
Ethanol	Soluplus	0.5	20	10:1	131 ± 12	0.22	−8.70 ± 1.35	22.45 ± 1.30
Ethanol	Soluplus	1	10	10:1	87 ± 5	0.21	−12.36 ± 1.21	20.50 ± 1.75
Ethanol	Soluplus	1	50	10:1	345 ± 34	0.34	−9.84 ± 1.24	-

Table 1. Optimization of Soluplus stabilized paclitaxel nanocrystals. **n = 3, Mean ± Standard Deviation.*

Nanocrystal: Lipid mixture	Lipid mixture					Peak	*Particle Size (nm)	PDI	*Zeta potential (mV)	*Drug payload (%)
	HSPC (mg)	Chol (mg)	TPGS (mg)	TPGS-COOH (mg)	Cmab					
1:2	60	60	15	-	-	Broad	171.0 ± 44.39	0.296	−7.84 ± 1.45	9.65 ± 2.10
1:2	60	40	15	-	-	Broad	156.9 ± 91.50	0.371	−8.23 ± 2.42	12.60 ± 2.83
1:2	60	30	15	-	-	Single	127.3 ± 56.3	0.364	−9.46 ± 2.01	11.79 ± 3.75
1:2	75	25	15	-	-	Broad	210.4 ± 68.40	0.350	−7.24 ± 1.90	10.75 ± 1.76
1:1	60	30	15	-	-	Single	139.70 ± 23.50	0.227	−11.08 ± 2.35`	**14.41 ± 1.29**
2:1	60	30	15	-	-	Broad bimodal	151.2 ± 50.26	0.63	−7.65 ± 0.57	-
1:1	60	30	7.5	7.5	+	Single	174.6 ± 31.73	0.268	−9.23 ± 1.90	**14.03 ± 2.83**

Table 2. Optimization of Lipid modified nanocrystals of paclitaxel. **n = 3, Mean ± Standard Deviation; Sign "+" means positive or present; Sign "-" means negative or absent.*

The antisolvent-to-solvent ratio of water to ethanol was also identified as an important process parameter. The 10:1 of antisolvent-to-solvent ratio was discovered appropriate for producing desirable nanocrystals. Although lower antisolvent to solvent ratios of 5:1 can increase nucleation rate, this impact is offset by nucleus growth due to the high solvent phase, resulting in larger crystals via Ostwald ripening[24,25]. At ratios greater than 10:1, no further drop in particle size was observed, presumably due to the reach of equilibrium state between drug nucleation and crystal growth[26]. However, a higher polydispersity index was observed. In summary, using 1% w/v Soluplus and PTX in a 10 ml aqueous antisolvent phase with 10:1 of antisolvent-to-solvent ratio was found suitable for producing stable PTX nanocrystals with a high payload. For optimization of lipid-modified nanocrystals, various formulations were prepared using varying ratios of HSPC: Chol and 'Nanocrystal: Lipid mixture' (Table 2). The ratio of 1:1 molar ratio of HSPC: Chol as lipid layer and 1:1 of nanocrystal: lipid mixture was optimal for obtaining lipid coated nanocrystals of desired size and high payload.

Physicochemical and microscopic characterization

The hydrodynamic size of Soluplus stabilized nanocrystals (PTX-NCs) was observed to be 109.30 ± 5.20 nm. The nanocrystals were homogeneously dispersed particulate system with PDI of 0.105 ± 0.027. The size of nanocrystals increased on lipid coating to give Lipid/PTX-NCs of size 139.70 ± 23.50 nm and PDI 0.227 ± 0.045. The cetuximab conjugation on nanocrystals further increased the size to 174.6 ± 31.73 nm and PDI 0.268 ± 0.036. However, nanocrystals were stable with a zeta potential of − 10.31 ± 1.82 mV, −11.08 ± 2.35 mV, and −9.23 ± 1.90

mV for PTX-NCs, Lipid/PTX-NCs and Cmab/Lipid/PTX-NCs, respectively. The drug content for PTX-NCs was about 26% attributed to nanocrystals with Soluplus stabilizer. While drug content for Lipid/PTX-NCs and Cmab/Lipid/PTX-NCs was about 14%. A decrease in overall drug content was observed probably due to the nanocrystals surface modification with phospholipids and cetuximab that increased the overall mass of nanocrystals. However, the drug content was still higher compared to conventional lipid-based nanoparticles[27]. Moreover, the PTX-NCs exhibited a yield of about 67.16 ± 5.18%. While, Lipid/PTX-NCs and Cmab/Lipid/PTX-NCs had a yield value of 85.05 ± 3.07% and 81.21 ± 2.09%, respectively.

The storage stability study also indicated high stability of nanocrystals, showing no significant change in particle size, PDI, and zeta potential over the period of 6 months (Fig. 2A). The formulations were also imaged by SEM, AFM, and TEM to confirm the surface morphology, shape and size of nanocrystals (Fig. 1A-I). SEM study revealed cube to rod-shaped nanocrystals with round edges of about 105.36 ± 11.79 nm for PTX-NCs and spherical particles of about 127.87 ± 24.507 nm for Lipid/PTX-NCs, and 165.31 ± 26.47 nm for Cmab/Lipid/PTX-NCs. The AFM assisted surface analysis of PTX-NCs and Lipid/PTX-NCs confirmed the smooth surfaced particles with size and shape, close to SEM results. The size observed in TEM was 102.27 ± 16.39 nm for PTX-NCs and 131.33 ± 21.23 nm for Lipid/PTX-NCs. The results were similar to the results observed in SEM and AFM. The increase in the size of Lipid/PTX-NCs compared to PTX-NCs was attributed to the lipid layer coating on the nanocrystal surfaces. The size of Cmab/Lipid/PTX-NCs was also higher (160.85 ± 36.14 nm) than Lipid/PTX-NCs due to cetuximab conjugation. The SAED pattern of all nanocrystals exhibited diffused rings, revealing the amorphous nature.

Solid state characterization

FTIR study was used to confirm the formation of PTX-NCs, Lipid/PTX-NCs, and Cmab/Lipid/PTX-NCs (Fig. 1.J). The characteristic peaks of pure PTX were observed at 1734.41 (C = O stretching vibration), 1646.91 (N = H bond), 1243.62 (C-N stretching), and 709.437 (C–C stretching). The physical mixture of pure PTX and Soluplus also exhibited peaks at 1733.63, 1646.42, 1244.82, and 710.15, similar to pure PTX but of decreased intensity. This confirmed the compatibility of drug with stabilizer[28]. In contrast, the sharp characteristics peaks of pure PTX were masked in PTX-NCs attributed to Soluplus coating on PTX. Additionally, Lipid/PTX-NCs followed the spectrum with merged trend of HSPC, Chol and TPGS (details in supplementary). Meanwhile, Cmab/Lipid/PTX-NCs showed peaks similar to Lipid/PTX-NCs. However, the disappearance of a peak at 1739.23 observed in the Lipid/PTX-NCs spectrum could be due to TPGS conjugation with cetuximab.

The XRD diffractograms of pure PTX as compared to physical mixture (SP-PM), PTX-NCs, Lipid/PTX-NCs, and Cmab/Lipid/PTX-NCs are shown in Fig. 1.K. The crystallinity of pure PTX was confirmed by the characteristic peaks at 2θ = 5.754, 9.100, 10.215, 11.367, 12.526, 14.044, 14.679, 15.760, 17.230, 18.096, 18.858, 19.650, 20.116, 21.0, 21.356, 22. 083, 22. 909, 25.353, 27.293, 28.792, 30.048, 32.982, and 34.380. The physical mixture of pure drug and Soluplus exhibited dominant peaks at 2θ = 5.645, 9.006, 10.139, 11.371, and 12.466. The peak broadening and reduction in peak intensity was due to surface coverage of crystalline drug with amorphous Soluplus dominating pure PTX peaks[28]. Additionally, the characteristic peaks of pure PTX were completely masked in PTX-NCs attributed to amorphization of crystalline PTX by Soluplus. Lipid/PTX-NCs exhibited peaks at 2θ = 5.581, 9.316, 14.430, 21.663, corresponding to lipid layer of HSPC, Chol and TPGS (details in supplementary). Cmab/Lipid/PTX-NCs also exhibited a diffraction pattern similar to Lipid/PTX-NCs but with reduced intensity, probably due to a similar composition with cetuximab surface modification.

DSC thermogram of pure PTX, physical mixture (SP-PM), PTX-NCs, Lipid/PTX-NCs, and Cmab/Lipid/PTX-NCs were also shown in Fig. 1.L. The endothermic peak observed by PTX at 223 °C corresponded to the melting of crystalline drug. While a low endothermic peak at 219 °C for the physical mixture was due to the physical interaction of PTX with Soluplus. In contrary, the endothermic peak of crystalline PTX was not present in PTX-NCs attributed to nanocrystals stabilization by Soluplus resulting in an amorphous molecular dispersion of drug. Lipid/ PTX-NCs and Cmab/Lipid/ PTX-NCs exhibited a prominent peak at 36 °C corresponding to TPGS, and the endothermic peak of PTX was still absent confirming lipid coating without affecting nanocrystals integrity and maintaining the drug in an amorphous state.

Degree of conjugation of cetuximab and surface chemistry

Bradford's assay confirmed the cetuximab conjugation on the surface of Lipid/PTX-NCs. The results showed a 68.2 ± 0.193% degree of Cmab conjugation on Lipid/PTX-NCs surface. This resulted in cetuximab of about 18.19 µg/mg of Lipid/PTX-NCs that may endow nanocrystals with targeting potential, similar to previous reports[29]. Using XPS, the Cmab conjugation was further confirmed with the elemental analysis of Lipid/PTX-NCs and Cmab/Lipid/PTX-NCs. XPS spectra revealed a change in the surface composition of Lipid/PTX-NCs on the conjugation of Cmab (Fig. 2B). A higher weight percentage contribution of nitrogen was observed in Lipid/PTX-NCs. Also, an additional peak of sulfur was observed in the case of Cmab/Lipid/PTX-NCs. Thus, the increase in nitrogen percentage and the presence of sulfur confirmed the successful conjugation of Cmab on the surface of nanocrystals.

In vitro drug release study

The role of surface-modified nanocrystals in drug release was determined by the dialysis bag method. Compared to pure PTX, Soluplus-stabilized (PTX-NCs) and lipid-coated (Lipid/PTX-NCs) nanocrystals had significantly higher drug release rates (Fig. 2C). Pure drug exhibited only 17% drug release in 24 h. While Soluplus stabilized nanocrystals showed almost complete drug release. The drug release was improved to five-fold by PTX-NCs as compared to free drug, avoiding the requirement of any external solubilizing agent like Cremophor EL. The increased drug release could be due to the higher dissolution velocity of nanocrystals. The lipid coating on PTX-NCs was found to control the drug release from nanocrystals. Lipid/PTX-NCs released only 57% drug in

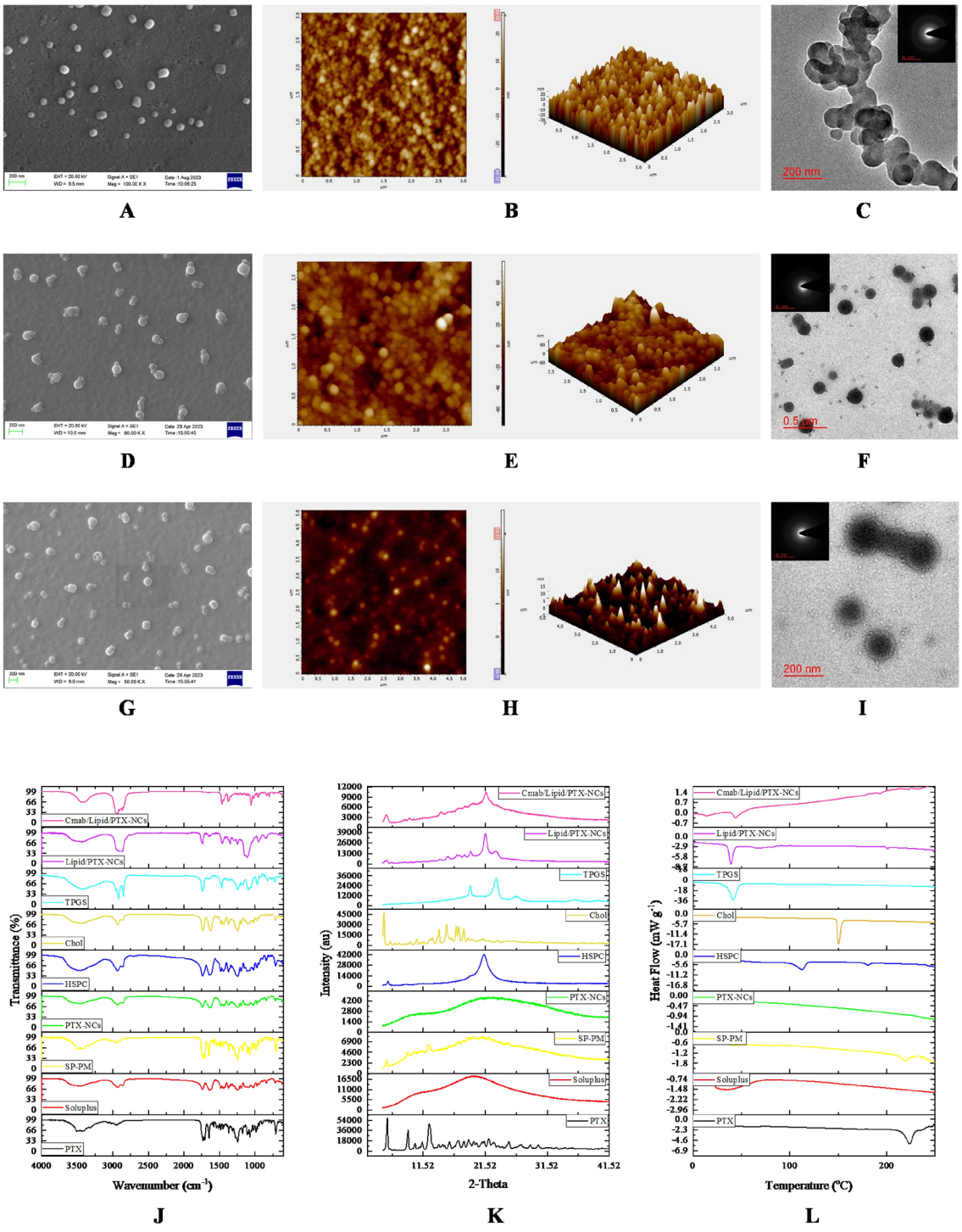

Fig. 1. Microscopic investigation of nanocrystals; SEM, AFM, and TEM images of PTX-NCs (**A**-**C**), Lipid/PTX-NCs (**D**-**F**), and Cmab/Lipid/PTX-NCs (**G**-**I**). Spectroscopic analysis including FTIR (**J**), XRD (**K**), and DSC (**L**) of PTX, Soluplus, PTX-NCs, HSPC, Chol, TPGS, Lipid/PTX-NCs, and Cmab/Lipid/PTX-NCs.

24h, attributed to phospholipid and TPGS coating on PTX-NCs surface responsible for slower dissolution and controlled release of drug from nanocrystals. Cetuximab functionalized lipid nanocrystals (Cmab/Lipid/PTX-NCs) also revealed slower drug release, similar to Lipid/PTX-NCs. Therefore, prepared lipid-coated nanocrystals were capable of controlling the drug release at pH 7.4, thereby prolonging the systemic circulation. The drug release was fitted to various release kinetics models (details in supplementary; Table S2). Pure PTX indicated low transport kinetic following Korsmeyer-Peppas ($n = 0.001$), Makoid-Banakar ($n = 0.646$, $k = 0.022$), and Weibull model ($\beta = 0.247$)[30]. The diffusion index n was 0.646 (i.e., $0.45 < n < 0.89$) as observed in the Makoid–Banakar model, suggesting drug release due to erosion as well as diffusion[7]. Therefore, the release of pure PTX was

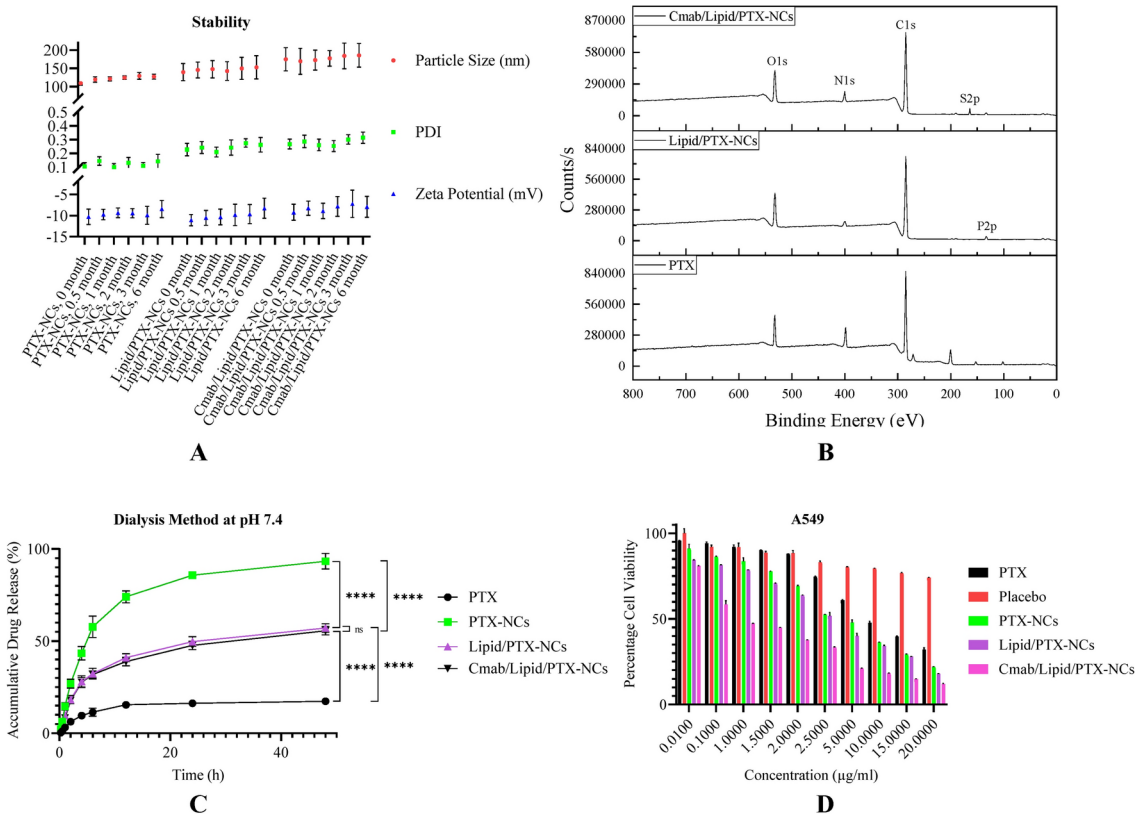

Fig. 2. Graphical representation of stability studies (**A**), XPS spectra (**B**) in-vitro drug release profile at 7.4 pH (**C**), and MTT assay in A549 cells (**D**).

erosion and diffusion-dependent and occurred in drugs with a slow-release rate[31]. The PTX-NCs were found to follow Weibull (β = 0.719), Logistic (β = 2.656), and Probit model (β = 1.572), showing diffusion-mediated drug release from colloidal particles[32–34]. The Weibull model's β value of 0.719 (i.e., β values below 0.75) confirmed faster drug release via diffusion mechanism[8]. The logistic and probit model suggested an initial higher release, probably due to the high dissolution of nanocrystals. In contrast, Lipid/PTX-NCs and Cmab/Lipid/PTX-NCs followed Korsmeyer-Peppas (n = 0.088 & 0.090), Weibull (β = 0.412 & 0.408), and Gompertz model (β = 0.847 & β = 0.823). The n value in Korsmeyer-Peppas was < 0.5, suggesting Quasi-Fickian diffusion (non-swellable matrix diffusion) from polymeric-controlled drug delivery systems[30,35]. Also, the β value observed in the Weibull and Gompertz model suggested drug release via Fickian and Gompertz diffusion for spherical particles[36,37]. The results suggested drug release from lipid nanocrystals similar to diffusion from nanoparticles or polymeric matrix systems[38].

In vitro cell line studies

Cell-cytotoxicity assay

To investigate the effect of pure PTX, PTX-NCs, Lipid/PTX-NCs, and Cmab/Lipid/PTX-NCs on lung cancer cells, cell viability was determined by MTT assay by treating A549 cells with different concentrations (0.01, 0.1, 1, 1.5, 2, 2.5, 5, 10, 15, and 20 µg/ml) for 48 h (Fig. 2D). The IC_{50} value of each treatment was calculated, where Cmab/Lipid/PTX-NCs showed the highest cytotoxicity at 1 µg/ml. Proliferation inhibition significantly increased with increasing paclitaxel concentration and thus exhibited cell cytotoxicity in a dose-dependent manner[39]. The pure PTX attenuated the cell viability to 49% at 10 µg/ml. Whereas PTX-NCs, Lipid/PTX-NCs, and Cmab/Lipid/PTX-NCs reduced cell viability to 36, 34, and 18%, respectively. The IC_{50} values for pure PTX, PTX-NCs, Lipid/PTX-NCs, and Cmab/Lipid/PTX-NCs were observed as 10.62, 5.9, 5.8, and 1.76, respectively. The higher efficacy of nanocrystals compared to pure PTX could be due to size-dependent and receptor-mediated uptake in cancer cells[40].

Nuclear morphological assessment through Hoechst 33342 /PI dual staining

After the cytotoxicity study, Hoechst 33342 and propidium iodide (H/PI) double staining method was used to investigate the cell death (cellular apoptosis). The morphological changes in the cell nuclei on treatment with pure PTX and nanocrystals was observed[41]. The nucleus-stained light blue (Hoechst 33342) was normal, pinkish red (PI staining) indicated late apoptotic/necrotic cells, while PI negative showed signs of early apoptosis. Live A549 cells exhibit cytoplasmic staining with large, oval-shaped, and evenly stained nuclei. While apoptotic cells can be identified with fragmented nuclei and condensed chromatin (apoptotic bodies)[42]. The morphological assessment revealed cell death due to apoptosis on treatment of A549 cells with pure PTX, PTX-NCs, Lipid/

PTX-NCs, and Cmab/Lipid/PTX-NCs (Fig. 3A). The control group exhibited homogeneous blue chromatin for normal nucleus morphology of live cells. However, pure PTX and NCs treated cells showed apoptotic nuclei linked to chromatin condensation as a result of PTX accumulation in cells. Additionally, nanocrystals were found to produce more apoptotic cells than pure PTX attributed to size and surface dependent endocytosis of nanocrystals[43]. Cmab/Lipid/PTX-NCs further increased the apoptosis as compared to PTX-NCs or Lipid/PTX-NCs probably due to cetuximab that endowed nanocrystals with the capability to enter cells through receptor mediated endocytosis[44]. The morphological observations revealed that maximum cells exhibited characteristics of apoptosis, showing shrinkage of cells, and a decrease in cell count[45]. Therefore, prominent morphological changes observed with surface-modified nanocrystals confirmed its role in inducing cellular apoptosis.

Mitochondrial membrane potential study through JC-1 staining

Change in mitochondrial membrane potential is linked to reactive oxygen species (ROS) generation[20]. ROS are largely produced by mitochondrial respiratory chain under PTX treatment, which results in a sharp decrease of the mitochondrial membrane potential. This results in oxidative stress responsible for oxidative damage to biomolecules (protein, lipids and DNA) and thus inducing apoptosis or necrosis[46]. Present work involved determination of variations in mitochondrial membrane potential by use of JC-1 dye (Fig. 3B). The control group showed red fluorescence due to the formation of j-aggregates (polarized). This suggested a higher mitochondrial membrane potential in the control group usually found in live cells. Contrary to this, green fluorescence (depolarization) was seen after treatment with pure PTX, indicating JC-1 dye binding with damaged mitochondria to form j-monomers. The nanocrystals exhibited more stronger green fluorescence than pure PTX, demonstrating their role in inducing higher apoptosis. Cmab/Lipid/PTX-NCs exhibited more stronger green fluorescence than Lipid/PTX-NCs and PTX-NCs. This could be due to induction of higher apoptosis by Cmab/Lipid/PTX-NCs as a result of receptor mediated internalization in cancer cells. Therefore, cetuximab-modified nanocrystals were more effective in inducing cellular apoptosis than non-targeted nanocrystals and pure PTX.

Cellular uptake study

The cellular uptake and intracellular tracking of free C6, C6-PTX-NCs, Lipid/C6-PTX-NCs, and Cmab/Lipid/C6-PTX-NCs was investigated in A549 cells using fluorescence microscope (Fig. 4A). The green fluorescence was tracked around the edges of the nucleus (blue fluorescence) in merged images. Compared to free C6, a higher green fluorescence was observed with nanocrystals, suggesting their accumulation dominantly in cytoplasmic regions of A549 cells. The lower fluorescence with C6 could be due to passively diffused C6 in cells that get eliminated at a faster rate by the p-gp efflux mechanism[41]. Also, strong fluorescence with nanocrystals could be due to their size and surface properties dependent on internalization in cells. Cmab/Lipid/PTX-NCs fluoresced higher than C6-PTX-NCs and Lipid/C6-PTX-NCs, showing enhanced accumulation of Cmab/Lipid/PTX-NCs in A549 cells attributed to receptor-mediated endocytosis and p-gp efflux inhibition[41,47].

Cell cycle analysis

The flowcytometry data analysis of placebo, pure PTX, PTX-NCs, Lipid/PTX-NCs, and Cmab/Lipid/PTX-NCs revealed differences in cell distribution across several phases of the cell cycle including Sub-G1 dead cells (M1), G0/G1 (M2), S phase (M3) and G2/M phase (M4) when compared to the control group (Fig. 4B). Histogram statistics showed that nanocrystals induced apoptosis (sub G1 percentage increase) in A549 cells[41]. Cell cycle analysis of the control group showed a higher percentage of G0/G1 phase and low G2/M phase, confirming cell proliferation. Treatment of cells with paclitaxel showed G2/M phase arrest (45.21%) and reduction in G0/G1 phase (18.99%), similar to previous reports[48]. This confirmed the paclitaxel-induced cell cycle arrest and cellular apoptosis[49]. Further, an increase in G2/M percentage and a decrease in G0/G1 percentage was observed with nanocrystals, probably due to their size-dependent internalization in cancer cells. The G2/M phase was around 52% after treatment with PTX-NCs and Lipid-PTX-NCs, while a higher percentage of 74.13% was observed with Cmab/Lipid/PTX-NCs treatment. The reduction in the percentage of cells in the G0/G1 phase and the increase in the G2/M phase is directly linked to mitotic arrest by PTX[47]. The findings suggested the role of nanocrystals in promoting cellular death while impeding cell cycle progression. Additionally, Cmab/Lipid/PTX-NCs were more effective in regulating cell growth as compared to non-targeted nanocrystals and pure PTX, demonstrating their superiority in the induction of cell cycle arrest and, thus, cellular apoptosis.

In vivo studies

Tumor regression, histological assessment and survival analysis

Tumor regression study was conducted in tumor bearing mice treated with pure PTX, PTX-NCs, Lipid/PTX-NCs, and Cmab/Lipid/PTX-NCs, compared to untreated tumor (control). The percentage change in body weight was determined in all treatment groups (Fig. 5A). PTX treated groups showed negative change in body weight probably due to toxic effects of drug. A significant increase in body weight was observed in untreated tumor bearing mice, however the weight not changed much on treatment with PTX-NCs, Lipid/PTX-NCs, and Cmab/Lipid/PTX-NCs. This could be due to ant-tumor effect as well as non-toxicity and high tolerability of prepared nanocrystals as per nanotoxicological classification system (NCS)[50]. The targeted nanocrystals (Cmab/Lipid/PTX-NCs) exhibited lowest change in body weight due to higher antitumor effect via receptor targeted drug delivery, than PTX-NCs and Lipid/PTX-NCs. Similar results were observed for cetuximab targeted lipid-nanoparticles due to higher tumor accumulation potential[27]. The histological assessment of lungs of pure PTX, PTX-NCs, Lipid/PTX-NCs, and Cmab/Lipid/PTX-NCs treated groups, compared to untreated tumor (control) was also done (Fig. 5B). The untreated tumor bearing mice had clear signs of proliferated tissue showing induction of lung cancer in mice. Pure PTX treated groups although had controlled the tumor growth but still

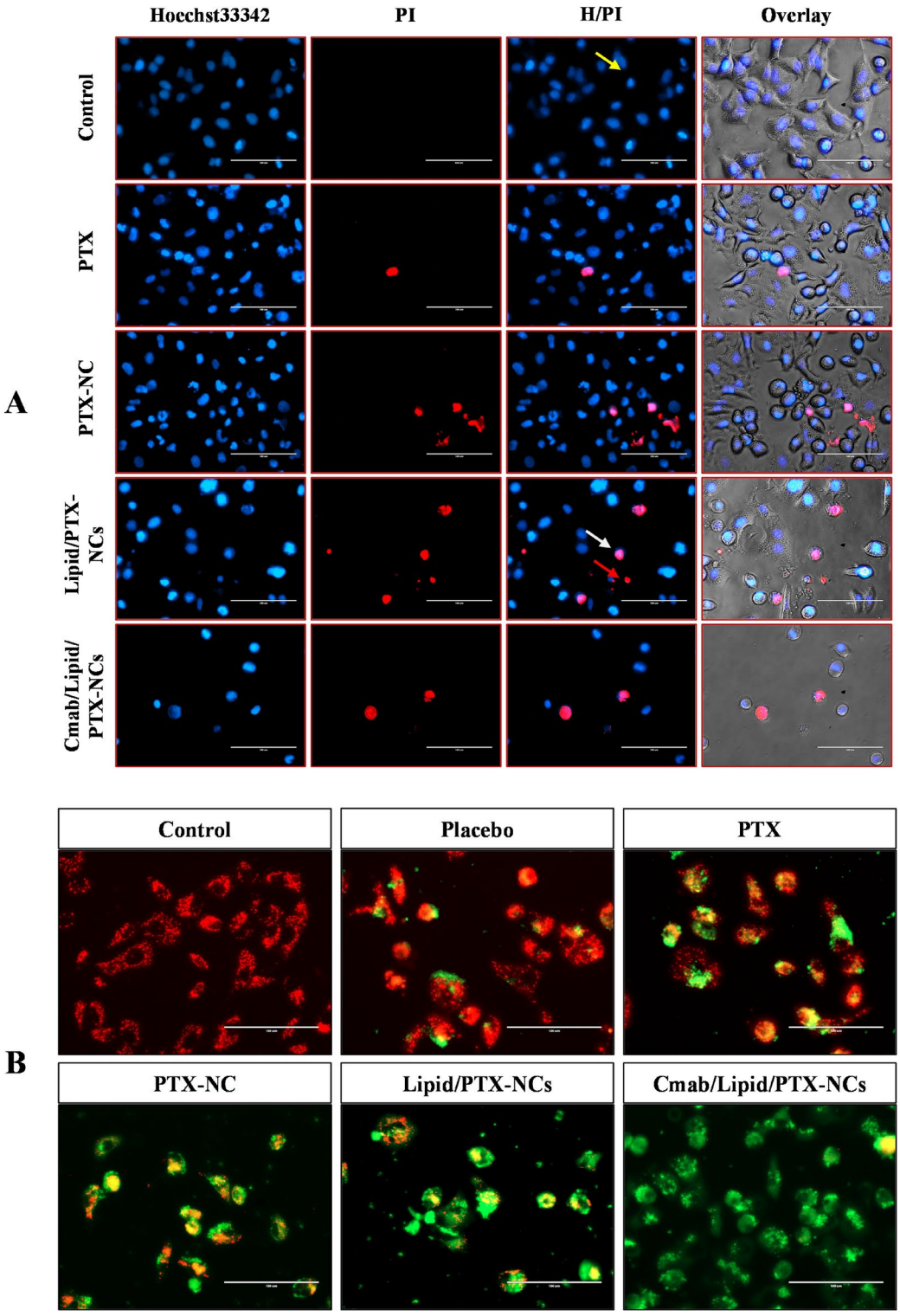

Fig. 3. (**A**) Nuclear morphological changes during apoptosis post-treatment to PTX, PTX-NCs, Lipid/PTX-NCs, and Cmab/Lipid/PTX-NCs, assessed through the Hoechst 33342/PI dual staining method. Yellow, white, and red arrows indicated live, early apoptotic, and late apoptotic cells, respectively. (**B**) Detection of mitochondrial membrane potential through JC-1 staining, green fluorescence was due to mitochondrial depolarization on treatment with PTX, PTX-NCs, Lipid/PTX-NCs, and Cmab/Lipid/PTX-NCs due to formation of j-monomers as a result of JC-1 dye binding with damaged mitochondria. Scale bar = 100μm.

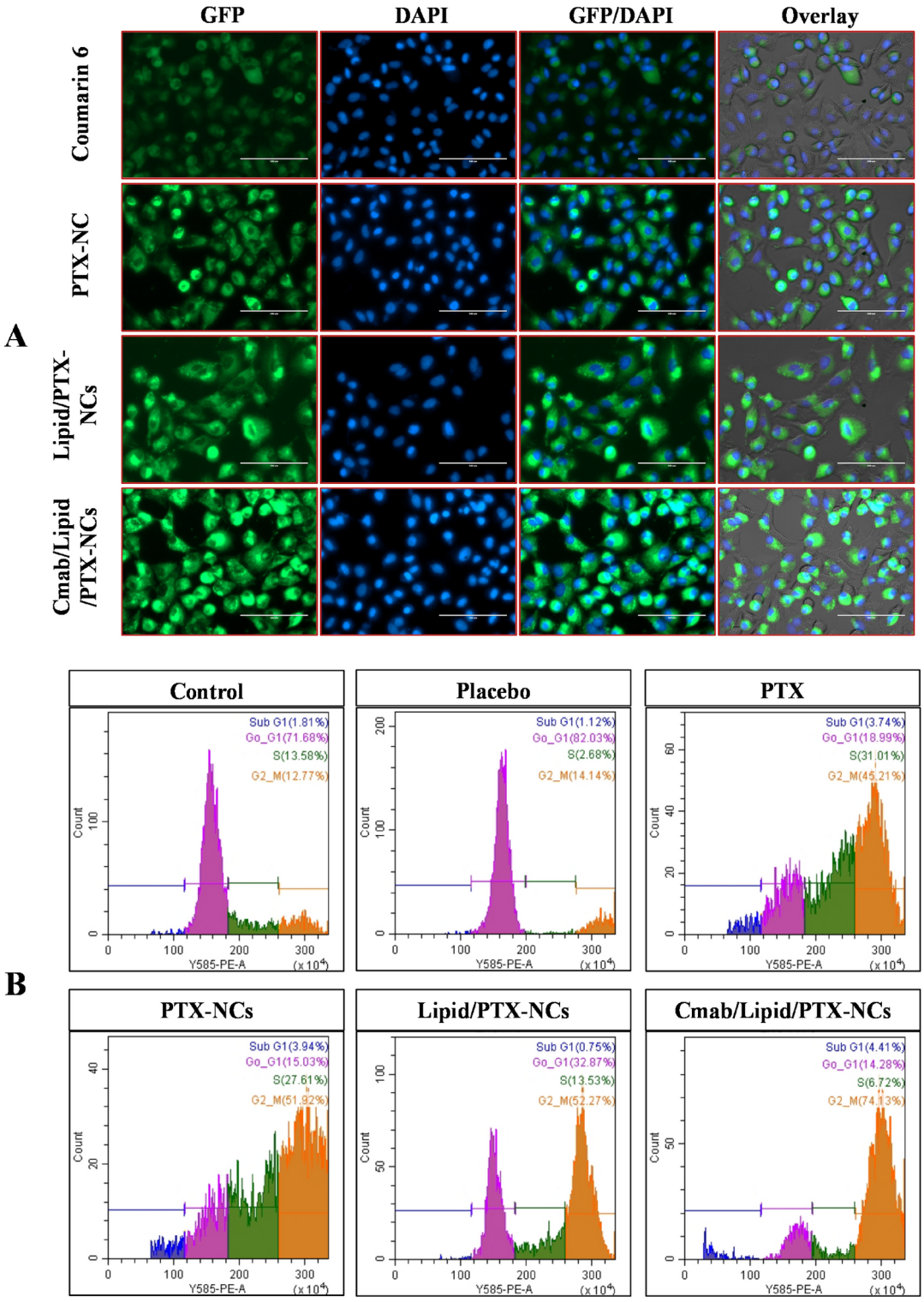

Fig. 4. (**A**) Fluorescence microscopic images of A549 cells showing cytoplasmic uptake of Free C6, pure PTX, PTX-NCs, Lipid/PTX-NCs, and Cmab/Lipid/PTX-NCs post 12 h of incubation. Cytoplasmic uptake showed green fluorescence and nuclear morphology was seen in blue fluorescence. Each scale bar represents 100 µm; (**B**) Quantitative cell cycle analysis showing different cell cycle stages (Sub G1, G1, S, and G2/M) of Control (untreated), Placebo formulation, pure PTX, PTX-NCs, Lipid/PTX-NCs, and Cmab/Lipid/PTX-NCs, through flow cytometry.

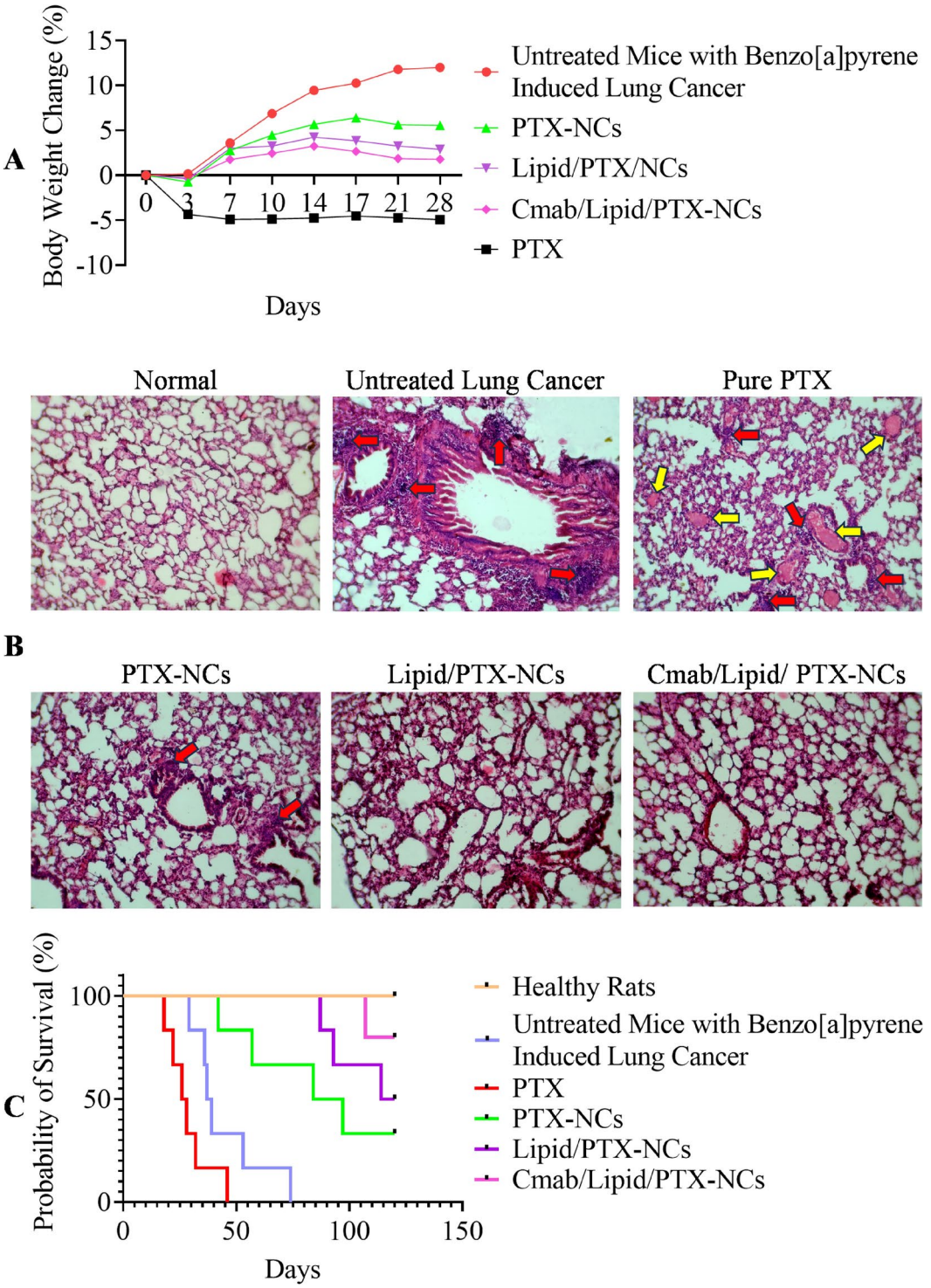

Fig. 5. (**A**) Change in body weight as a response to intravenous administration of pure PTX, PTX-NCs, Lipid/PTX-NCs, and Cmab/Lipid/PTX-NCs in mice with Benzo[a] pyrene-induced lung cancer; (**B**) The histological assessment of lungs of pure PTX, PTX-NCs, Lipid/PTX-NCs, and Cmab/Lipid/PTX-NCs treated groups, compared to Normal healthy mice and untreated mice (Benzo[a]pyrene induced lung cancer model); (**C**) Kaplan–Meier survival probability plot of Normal healthy mice, untreated mice (Benzo[a]pyrene induced lung cancer model) and mice having benzo[a]pyrene induced lung cancer model treated with pure PTX, PTX-NCs, Lipid/PTX-NCs, and Cmab/Lipid/PTX-NCs.

had visible signs of cancer cell proliferation. PTX-NCs and Lipid/PTX-NCs found to control the tumor growth, however the density was still high with few cancer cells remain. Cmab/Lipid/PTX-NCs revealed the morphology similar to normocellular histology, and thus was capable of treating the lung tumor effectively. The survival analysis further showed prolonged survival of PTX-NCs, Lipid/PTX-NCs, and Cmab/Lipid/PTX-NCs treated groups compared to pure PTX treated groups (Fig. 5C). Th mean survival of untreated control, Pure PTX, PTX-NCs, Lipid/PTX-NCs, and Cmab/Lipid/PTX-NCs groups were 38, 27, 90.5, 117, and > 120 days, respectively. The lower survival of pure PTX, treated group was due to toxic effects of drug. While, improved survival of nanocrystals was attributed to their role in tumor growth inhibition and minimized toxic effects[51].

Pharmacokinetics and biodistribution study

The pharmacokinetic study was conducted for intravenously administered pure PTX, PTX-NCs, Lipid/PTX-NCs, and Cmab/Lipid/PTX-NCs. The plasma concentration of PTX-NCs, Lipid/PTX-NCs, and Cmab/Lipid/PTX-NCs was significantly higher than pure PTX (Fig. 6). Formulation of drug as nanocrystals decreased the clearance rate, increased the half-life and improved the mean retention time of Lipid/PTX-NCs, and Cmab/Lipid/PTX-NCs compared to PTX-NCs and pure PTX (Table 3). This could be due to TPGS and phospholipid coating on the nanocrystals' surface responsible for prolonging the systemic circulation[52]. The nanocrystals also exhibited a higher Cmax and AUC than pure PTX; thus, more drugs were available for distribution to the target site.

The study was also conducted to determine the effect of surface-modified nanocrystals on organ distribution (Fig. 6). Free PTX gets distributed to all the major organs, including the lungs, liver, kidney, spleen, and brain. At 0.5 h, free PTX gets distributed to the heart, kidneys, and liver at a significantly (****) higher concentration. The distribution in the lung was significantly (***) improved by Cmab/Lipid/PTX-NCs attributed to cetuximab targeted drug delivery. At 1 h, lung distribution by free PTX was also significantly lower than Lipid/PTX-NCs and Cmab/Lipid/PTX-NCs but exhibited significantly higher distribution in other organs. The lung distribution at 6 h and 12 h by Cmab/Lipid/PTX-NCs was significantly higher than Lipid/PTX-NCs (*) and PTX-NCs (****) and free PTX (****). Overall, the drug distribution by nanocrystals to other organ except lungs was significantly lower as compared to free PTX. The higher distribution of nanocrystals to lungs could be due to the enhanced permeation and retention effect of nanocrystals by exploiting loose vasculature in sites of lung cancer[18]. Furthermore, the higher distribution to the lung by Cmab/Lipid/PTX-NCs compared to Lipid/PTX-NCs and PTX-NCs and free PTX was attributed to cetuximab-mediated receptor-targeted delivery in lung cancers. The pharmacokinetic parameters determined using lung plasma concentration–time profile also confirmed higher cellular bioavailability of the drug by Cmab/Lipid/PTX-NCs followed by Lipid/PTX-NCs and PTX-NCs, as compared to free PTX (Table 3).

Conclusion

The present work showed the fabrication of phospholipid-modified and cetuximab-conjugated nanocrystals for drug delivery to cancer. The nanocrystals were homogeneous and stable, with particle sizes below 200 nm. Spectroscopic analysis confirmed the conversion of crystalline drugs to amorphous particles when fabricated as nanocrystals. The successful lipid modification and cetuximab conjugation on the nanocrystal surface was also observed. In-vitro cell line studies confirmed the role of nanocrystals in exerting higher cytotoxicity in A549 cancer cells and inducing cellular apoptosis by improving cellular uptake of PTX and providing cell cycle arrest at G2/M phase, all together responsible for higher antitumor efficacy of nanocrystals in A549 cells, as evidenced by reduced IC_{50} values. The in vivo studies revealed the nanocrystal's potency in controlling tumor growth, prolonging the survival period, and lowering PTX toxicity to give a safer medicine for cancer therapy. The results revealed phospholipid modified and cetuximab conjugated nanocrystals as a novel nanocarrier for site specific drug delivery and cancer therapy.

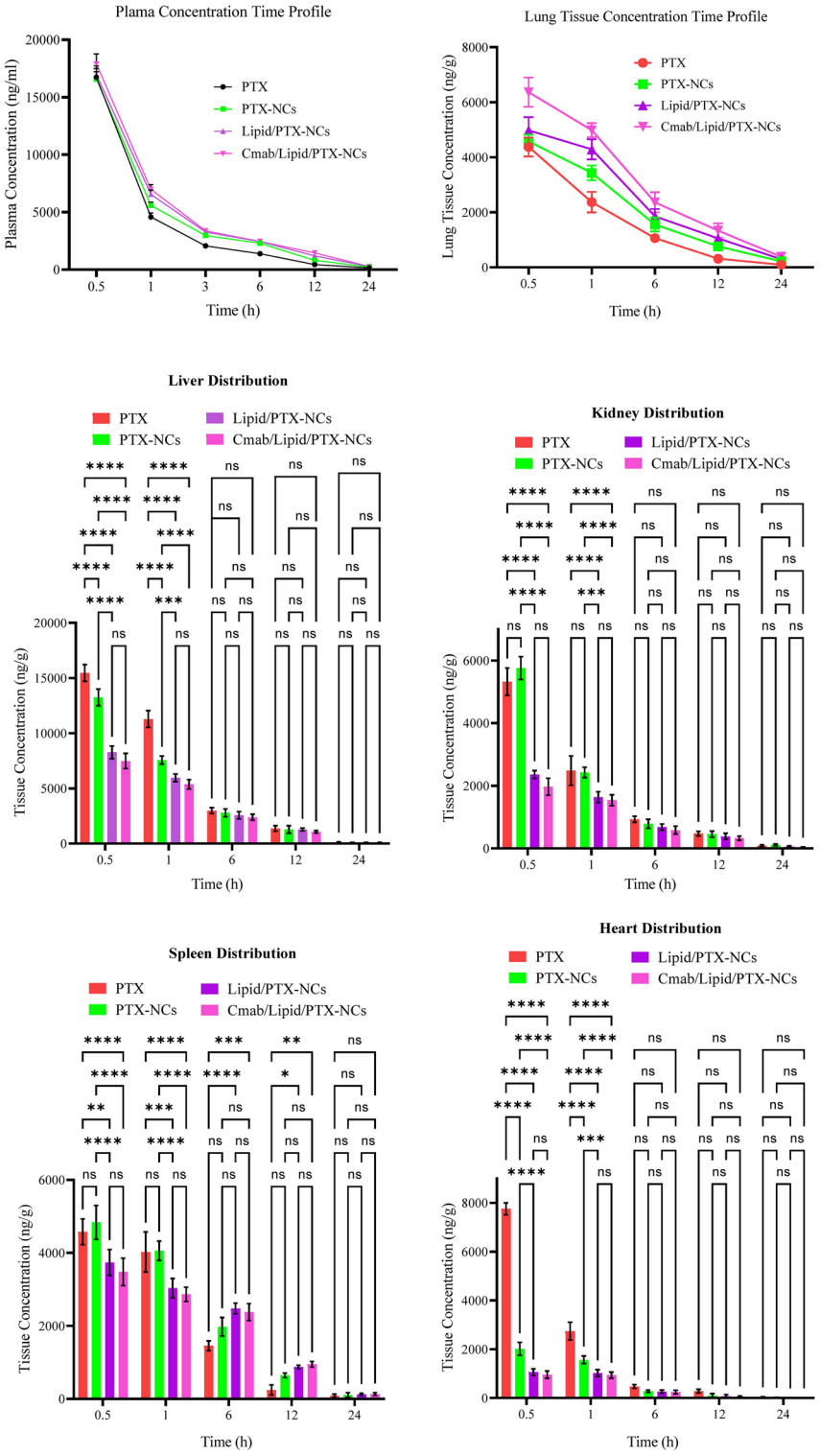

Fig. 6. Drug distribution in plasma and major organs including brain, heart, kidney, spleen, liver and lung on intravenous administration of PTX, PTX-NCs, Lipid/PTX-NCs, and Cmab/Lipid/PTX-NCs.

Parameters	pure PTX	PTX-NCs	Lipid/PTX-NCs	Cmab/Lipid/PTX-NCs
Pharmacokinetic parameters for plasma concentration–time profile				
$t_{1/2}$ (h)	4.695 ± 0.061	5.492 ± 0.0168	5.620 ± 0.0588	5.803 ± 0.1390
$C_{0.5}$ (ng/mL)	16,744 ± 758.755	16,575 ± 647.86	16,967 ± 755.86	17,898 ± 865.76
AUC_{0-t} (ng/mL.h)	45,750.9 ± 1682.195	53,925.19 ± 1609.47	61,385.39 ± 2016.207	65,712.59 ± 2616.405
MRT (h)	3.753 ± 0.023	4.865 ± 0.017	5.540 ± 0.014	5.730 ± 0.0616
Pharmacokinetic parameters for Lung tissue concentration–time profile				
$t_{1/2}$ (h)	4.721 ± 1.232	6.361 ± 0.095	6.746 ± 0.011	6.821 ± 0.233
Tmax (h)	0.5 ± 0	0.5 ± 0	0.5 ± 0	0.5 ± 0
C_{max} (ng/g)	4374 ± 346.7	4577 ± 246.7	4978 ± 477.80	6366 ± 536.80
AUC_{0-t} (ng/g.h)	17,984.25 ± 3033.965	30,471.32 ± 3382.581	38,622.57 ± 4094.966	48,080.97 ± 6104.766
MRT (h)	5.965 ± 1.246	7.924 ± 0.221	8.476 ± 0.075	8.781 ± 0.173

Table 3. Pharmacokinetic parameters for intravenous administered free PTX, PTX-NCs, Lipid/PTX-NCs, and Cmab/Lipid/PTX-NCs**.**

Data availability

All data generated or analysed during this study are included in this published article [and its supplementary information files].

Received: 5 June 2024; Accepted: 18 November 2024
Published online: 24 November 2024

References

1. Wen, G. et al. Recent advances in design, synthesis and bioactivity of paclitaxel-mimics. *Fitoterapia* **110**, 26–37 (2016).
2. Tong, Y., Luo, Y. F. & Gao, W. Biosynthesis of paclitaxel using synthetic biology. *Phytochem. Rev.* **21**, 863–877 (2022).
3. Haddad, R., Alrabadi, N., Altaani, B. & Li, T. Paclitaxel Drug Delivery Systems: Focus on Nanocrystals' Surface Modifications. *Polymers* **14**, 658 (2022).
4. Miele, E., Spinelli, G. P., Miele, E., Tomao, F. & Tomao, S. Albumin-bound formulation of paclitaxel (Abraxane® ABI-007) in the treatment of breast cancer. *Int. J. Nanomedicine* **4**, 99–105 (2009).
5. Joshi, R., Gore, A. Y., Rubinfeld, J. & Shrotriya, R. Oral formulation for paclitaxel. (2001).
6. ten Tije, A. J., Verweij, J., Loos, W. J. & Sparreboom, A. Pharmacological Effects of Formulation Vehicles. *Clin. Pharmacokinet.* **42**, 665–685 (2003).
7. Gigliobianco, M. R., Casadidio, C., Censi, R. & Di Martino, P. Nanocrystals of Poorly Soluble Drugs: Drug Bioavailability and Physicochemical Stability. *Pharmaceutics* **10**, 134 (2018).
8. Patel, A. et al. Nanocrystals: an emerging paradigm for cancer therapeutics. *Future J. Pharm. Sci.* **10**, 4 (2024).
9. Kumar, M., Jha, A., Bharti, K., Manjit & Mishra, B. Fucoidan-based bosutinib nanocrystals for pulmonary drug delivery: Solid state characterization and *in-vitro* assessment. *Chem. Phys. Impact* **8**, 100644 (2024).
10. Bonhoeffer, B., Kordikowski, A., John, E. & Juhnke, M. Numerical modeling of the dissolution of drug nanocrystals and its application to industrial product development1. *ADMET DMPK* **10**, 253–287 (2022).
11. Manish, K., Nithya, S. & Rajnikanth, P. S. Authors review on drug nanocrystals: a progress to targeted delivery. *Curr Nanomed* **10**, 1–23 (2020).
12. Park, J., Sun, B. & Yeo, Y. Albumin-coated nanocrystals for carrier-free delivery of paclitaxel. *J. Control. Release Off. J. Control. Release Soc.* **263**, 90–101 (2017).
13. He, Y. et al. Reducing systemic absorption and macrophages clearance of genistein by lipid-coated nanocrystals for pulmonary delivery. *Chin. Chem. Lett.* **34**, 107484 (2023).
14. Kumar, M. et al. Lipid-coated nanocrystals of paclitaxel as dry powder for inhalation: Characterization, in-vitro performance, and pharmacokinetic assessment. *Colloids Surf. B Biointerfaces* **237**, 113865 (2024).
15. Zhang, H. et al. pH-responsive lipid polymer hybrid nanoparticles (LPHNs) based on poly (β-amino ester) as a promising candidate to resist breast cancers. *J. Drug Deliv. Sci. Technol.* **61**, 102102 (2021).
16. Jha, A. *et al.* Hyaluronic acid-oleylamine and chitosan-oleic acid conjugate-based hybrid nanoparticle delivery via. dissolving microneedles for enhanced treatment efficacy in localized breast cancer. *Biomater. Adv.* **160**, 213865 (2024).
17. Lu, Y. et al. Development and evaluation of transferrin-stabilized paclitaxel nanocrystal formulation. *J. Controlled Release* **176**, 76–85 (2014).
18. Zhang, H., Hollis, C. P., Zhang, Q. & Li, T. Preparation and antitumor study of camptothecin nanocrystals. *Int. J. Pharm.* **415**, 293–300 (2011).
19. Khramtsov, P. et al. Measuring the concentration of protein nanoparticles synthesized by desolvation method: Comparison of Bradford assay, BCA assay, hydrolysis/UV spectroscopy and gravimetric analysis. *Int. J. Pharm.* **599**, 120422 (2021).
20. Shah, A. & Dobrovolskaia, M. A. Detection of Nanoparticle-Mediated Change in Mitochondrial Membrane Potential in T Cells Using JC-1 Dye. in *Characterization of Nanoparticles Intended for Drug Delivery* (eds. Clogston, J. D., Crist, R. M., Dobrovolskaia, M. A. & Stern, S. T.) 153–159 (Springer US, New York, NY, 2024). https://doi.org/10.1007/978-1-0716-3786-9_16.
21. Hassan, S. K. et al. Antitumor activity of *Cuphea ignea* extract against benzo(a)pyrene-induced lung tumorigenesis in Swiss Albino mice. *Toxicol. Rep.* **6**, 1071–1085 (2019).
22. Kumar, M., Shanthi, N., Mahato, A. K., Soni, S. & Rajnikanth, P. S. Preparation of luliconazole nanocrystals loaded hydrogel for improvement of dissolution and antifungal activity. *Heliyon* **5**, e01688 (2019).
23. Zhang, J.-Y. et al. Preparation of amorphous cefuroxime axetil nanoparticles by controlled nanoprecipitation method without surfactants. *Int. J. Pharm.* **323**, 153–160 (2006).
24. Sinha, B., Müller, R. H. & Möschwitzer, J. P. Bottom-up approaches for preparing drug nanocrystals: Formulations and factors affecting particle size. *Int. J. Pharm.* **453**, 126–141 (2013).
25. Kumar, M., Shanthi, N. & Mahato, A. K. Pharmaceutical Drug Nanocrystals: Role in Dermal Delivery. *Nanosci. Nanotechnol.-Asia* **9**, 300–310.

26. Zhao, H. et al. Facile Preparation of Danazol Nanoparticles by High-Gravity Anti-solvent Precipitation (HGAP) Method. *Chin. J. Chem. Eng.* **17**, 318–323 (2009).
27. Guo, S. et al. Synergistic combination therapy of lung cancer: Cetuximab functionalized nanostructured lipid carriers for the co-delivery of paclitaxel and 5-Demethylnobiletin. *Biomed. Pharmacother.* **118**, 109225 (2019).
28. Sharma, M. & Mehta, I. Surface stabilized atorvastatin nanocrystals with improved bioavailability, safety and antihyperlipidemic potential. *Sci. Rep.* **9**, 16105 (2019).
29. El Hallal, R., Lyu, N. & Wang, Y. Effect of Cetuximab-Conjugated Gold Nanoparticles on the Cytotoxicity and Phenotypic Evolution of Colorectal Cancer Cells. *Molecules* **26**, 567 (2021).
30. Olejnik, A., Kapuscinska, A., Schroeder, G. & Nowak, I. Physico-chemical characterization of formulations containing endomorphin-2 derivatives. *Amino Acids* **49**, 1719–1731 (2017).
31. Papadopoulou, V., Kosmidis, K., Vlachou, M. & Macheras, P. On the use of the Weibull function for the discernment of drug release mechanisms. *Int. J. Pharm.* **309**, 44–50 (2006).
32. Craciun, A.-M., Barhalescu, M. L., Agop, M. & Ochiuz, L. Theoretical Modeling of Long-Time Drug Release from Nitrosalicyl-Imine-Chitosan Hydrogels through Multifractal Logistic Type Laws. *Comput. Math. Methods Med.* **2019**, 4091464 (2019).
33. Ghosal, K., Chandra, A., Rajabalaya, R., Chakraborty, S. & Nanda, A. Mathematical modeling of drug release profiles for modified hydrophobic HPMC based gels. *Pharm.- Int. J. Pharm. Sci.* **67**, 147–155 (2012).
34. Corsaro, C., Neri, G., Mezzasalma, A. M. & Fazio, E. Weibull Modeling of Controlled Drug Release from Ag-PMA Nanosystems. *Polymers* **13**, 2897 (2021).
35. Siepmann, J. & Peppas, N. A. Higuchi equation: Derivation, applications, use and misuse. *Int. J. Pharm.* **418**, 6–12 (2011).
36. Martín-Camacho, U. de J., Rodríguez-Barajas, N., Sánchez-Burgos, J. A. & Pérez-Larios, A. Weibull β value for the discernment of drug release mechanism of PLGA particles. *Int. J. Pharm.* **640**, 123017 (2023).
37. Zhang, S., Fan, X., Zhang, G., Wang, W. & Yan, L. Preparation, characterization, and in vitro release kinetics of doxorubicin-loaded magnetosomes. *J. Biomater. Appl.* **36**, 1469–1483 (2022).
38. Sarveswari, H. B., Gupta, K. K., Durai, R. & Solomon, A. P. Development of a smart pH-responsive nano-polymer drug, 2-methoxy-4-vinylphenol conjugate against the intestinal pathogen. *Vibrio cholerae. Sci. Rep.* **13**, 1250 (2023).
39. Zheng, W. & Xu, S. Analysis of Differential Expression Proteins of Paclitaxel-Treated Lung Adenocarcinoma Cell A549 Using Tandem Mass Tag-Based Quantitative Proteomics. *OncoTargets Ther.* **13**, 10297 (2020).
40. Augustine, R. et al. Cellular uptake and retention of nanoparticles: Insights on particle properties and interaction with cellular components. *Mater. Today Commun.* **25**, 101692 (2020).
41. Singh, R. P. et al. Vitamin E TPGS conjugated carbon nanotubes improved efficacy of docetaxel with safety for lung cancer treatment. *Colloids Surf. B Biointerfaces* **141**, 429–442 (2016).
42. Pang, Z., Bondada, V., Sengoku, T., Siman, R. & Geddes, J. W. Calpain Facilitates the Neuron Death Induced by 3-Nitropropionic Acid and Contributes to the Necrotic Morphology. *J. Neuropathol. Exp. Neurol.* **62**, 633–643 (2003).
43. Rennick, J. J., Johnston, A. P. R. & Parton, R. G. Key principles and methods for studying the endocytosis of biological and nanoparticle therapeutics. *Nat. Nanotechnol.* **16**, 266–276 (2021).
44. Wang, Y., Huang, H.-Y., Yang, L., Zhang, Z. & Ji, H. Cetuximab-modified mesoporous silica nano-medicine specifically targets EGFR-mutant lung cancer and overcomes drug resistance. *Sci. Rep.* **6**, 25468 (2016).
45. Ramadoss, D. P. & Sivalingam, N. Vanillin extracted from proso and barnyard millets induces cell cycle inhibition and apoptotic cell death in MCF-7 cell line. *J. Cancer Res. Ther.* **17**, 1425 (2021).
46. Zhang, Y. et al. Paclitaxel Induces the Apoptosis of Prostate Cancer Cells via ROS-Mediated HIF-1α Expression. *Molecules* **27**, 7183 (2022).
47. Singh, R. P. et al. Chitosan-folate decorated carbon nanotubes for site specific lung cancer delivery. *Mater. Sci. Eng. C* **77**, 446–458 (2017).
48. Zhu, Z. et al. Modulation of alternative splicing induced by paclitaxel in human lung cancer. *Cell Death Dis.* **9**, 1–12 (2018).
49. Zhou, H., Liu, C., Yu, S., Shafiq, F. & Qiao, W. Paclitaxel solubilized nanoparticles based on binding affinity for efficient drug delivery. *J. Mol. Liq.* **389**, 122936 (2023).
50. Müller, R. H., Shegokar, R., Gohla, S. & Keck, C. M. Nanocrystals: Production, Cellular Drug Delivery, Current and Future Products. in *Intracellular Delivery: Fundamentals and Applications* (ed. Prokop, A.) 411–432 (Springer Netherlands, Dordrecht, 2011). https://doi.org/10.1007/978-94-007-1248-5_15.
51. Hollis, C. P. et al. Biodistribution and bioimaging studies of hybrid paclitaxel nanocrystals: lessons learned of the EPR effect and image-guided drug delivery. *J. Controlled Release* **172**, 12–21 (2013).
52. Farooq, M. A. & Trevaskis, N. L. TPGS Decorated Liposomes as Multifunctional Nano-Delivery Systems. *Pharm. Res.* **40**, 245–263 (2023).

Acknowledgements

Authors gratefully acknowledge Ministry of Education, Govt. of India and IIT (BHU), Varanasi, India for providing teaching assistantship. Authors are thankful to Central Instrumentation Facility (CIF) IIT(BHU), Varanasi and SATHI-BHU, Varanasi for providing the instrumental support.

Author contributions

M.K. conceptualizes the experiment; M.K. conceived the experiment, and together with P.G. and A.J. carried it out; M.K., P.G. and A.J. designed and carried out the data analysis; M.K. and P.G. co-wrote the paper; M.M. and AP.S. prepared figures; B.M. and B.K. supervised the experiment and did review-editing; All authors reviewed the manuscript.

Declarations

Competing interests

The authors declare no competing interests.

Additional information

Supplementary Information The online version contains supplementary material available at https://doi.org/10.1038/s41598-024-80283-8.

Correspondence and requests for materials should be addressed to B.K. or B.M.